Noname manuscript No.
(will be inserted by the editor)

Explicit expressions for the estimation of the elastic constants of lamellar bone as a function of the volumetric mineral content using a multiscale approach

Ana Vercher-Martínez · Eugenio Giner · Ricardo Belda · Abdelmalik Aigoun · F. Javier Fuenmayor

Received: date / Accepted: date

Abstract In this work, explicit expressions to estimate all the transversely isotropic elastic constants of lamellar bone as a function of the volumetric bone mineral density (BMD) are provided. The methodology presented is based on the direct homogenization procedure using the finite element method, the con-

A. Vercher-Martínez (✉) · E. Giner · R. Belda · F. J. Fuenmayor

Centro de Investigación en Ingeniería Mecánica - CIIM,

Depto. de Ingeniería Mecánica y de Materiales,

Universitat Politècnica de València, Camino de Vera, 46022 Valencia, Spain

E-mail: anvermar@dimm.upv.es

A. Aigoun

University Pierre et Marie Curie,

4 Place Jussieu, 75005 Paris, France

tinuum approach based on the Hill bounds, the least-square method and the mean field technique. Firstly, a detailed description of the volumetric content of the different components of bone is provided. The parameters defined in this step are related to the volumetric bone mineral density (BMD) considering that bone mineralization process occurs at the smallest scale length of the bone tissue. Then, a thorough description provides the details of the numerical models and the assumptions adopted to estimate the elastic behavior of the forward scale lengths. The results highlight the noticeable influence of the BMD on the elastic modulus of lamellar bone. Power law regressions fit the Young's moduli, shear stiffness moduli and Poisson ratios. In addition, the explicit expressions obtained are applied to the estimation of the elastic constants of cortical bone. At this scale length, a representative unit cell of cortical bone is analyzed including the fibril orientation pattern given by Wagermaier et al. (2006) and the BMD distributions observed by Granke et al. (2013) for the osteon. Results confirm that fibril orientation arrangement governs the anisotropic behavior of cortical bone instead of the BMD distribution. The novel explicit expressions obtained in this work can be used for improving the accuracy of bone fracture risk assessment.

Keywords Lamellar bone · Elastic constants · Volumetric bone mineral density · Multi-scale approach

1 INTRODUCTION

The assessment of fracture risk based on bone mineral density only is not enough for predicting bone fracture (Ulrich et al., 1999; Roque et al., 2013; Yang et al., 2014). This motivates the additional consideration of the apparent elastic properties of bone besides morphological parameters as other factors also determinant in the structural competence of bone (Roque et al., 2013). Numerical models of bone can be created from segmented μCT (micro computed tomography) images, and analyzed to obtain the apparent elastic constants of bone structure. In this process, it is necessary to assign material properties to the bone tissue and that is not a trivial issue. Usually, no direct influence of the mineral content is taken into account and typical isotropic elastic constants are considered (Ulrich et al., 1998; Roque et al., 2013; Daszkiewicz et al., 2017).

Many authors have reported that a little increase in the mineral content of bone has a direct consequence on the increase of its stiffness (Currey, 1986, 1988; Schaffler et al., 1988; Hernández et al., 2001a; Tommasini and Landis, 2008). In fact, some researchers have worked on the development of models that include the mineral content in the estimations of elastic properties of bone. In Currey (1986), a power law for the relationship between the BMD and the apparent elastic modulus of cancellous bone is reported. In Martínez-Reina et al. (2011) a micromechanical multi-scale model is presented for calculating the Young's moduli of cortical bone as a function of porosity and mineral content represented by the ash fraction. In that work, a detailed review of

previous models can also be found. Nevertheless, the volumetric BMD map can be obtained by dual-energy X-ray absorptiometry (DXA) (Yu et al., 1998; Yang et al., 2014) or quantitative computed tomography (QCT) (Yu et al., 1998; Grampp et al. , 1997; Majumdar et al., 1998; Barbour, 2010) in the usual clinical practice instead of the ash fraction. In addition, there are significant differences in BMD at the different skeletal sites and ages (Majumdar et al., 1998; Barbour, 2010). To the authors' knowledge, no explicit expressions have been proposed for the estimation of the full stiffness matrix of lamellar tissue as a function of the volumetric bone mineral density.

Results from a previous work of the authors (Vercher-Martínez et al., 2015) have been considered as starting point. In that work, a study about the influence of the geometrical mineral staggering on the elastic properties of the mineralized collagen fibril was performed. These results concern exclusively the transversely isotropic fibril assembly (fibres). In that work, no relation between volumetric mineral fraction and Bone Mineral Density (BMD) was established, extra-fibrilar matrix was not included and no higher scale level in the hierarchical structure of bone was addressed. In the present work, all these limitations have been overcome.

The main goal of this work is to provide explicit expressions for the estimation of all the elastic constants of lamellar bone as a function of the volumetric bone mineral density.

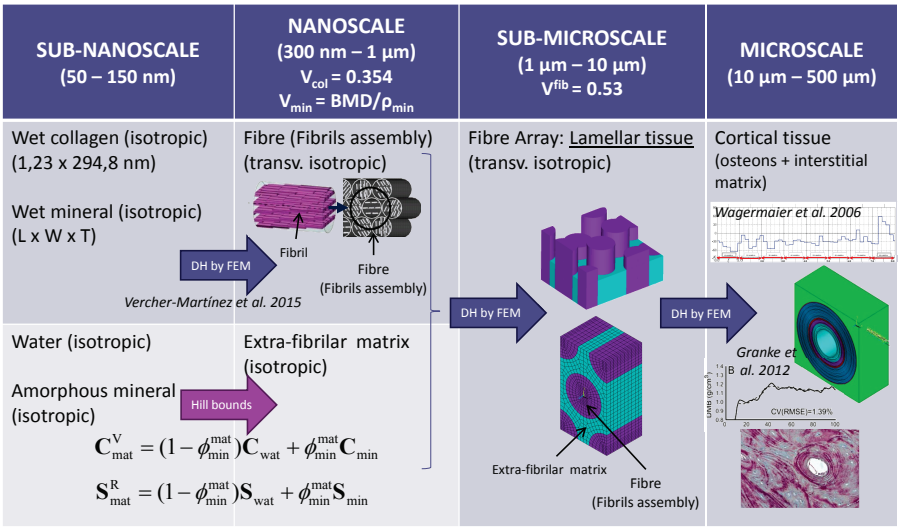

$$\mathbf{C}^{\mathrm{V}}_{\mathrm{mat}} = (1-\phi^{\mathrm{mat}}_{\mathrm{min}})\mathbf{C}_{\mathrm{wat}} + \phi^{\mathrm{mat}}_{\mathrm{min}}\mathbf{C}_{\mathrm{min}}$$

$$\mathbf{S}^{\mathrm{R}}_{\mathrm{mat}} = (1-\phi^{\mathrm{mat}}_{\mathrm{min}})\mathbf{S}_{\mathrm{wat}} + \phi^{\mathrm{mat}}_{\mathrm{min}}\mathbf{S}_{\mathrm{min}}$$

Fig. 1 Summary scheme of the multiscale approach performed in the current work

In Sec. 2 a thorough explanation of the multi-scale approach is given. In Sec. 3 the target expressions and other relevant results are provided. Finally the conclusions and future works are presented in Sec. 4.

2 METHODS

2.1 Introduction

Considering the hierarchical structure of bone (Hamed et al., 2012), the workflow of the multiscale approach followed in this work is depicted in Fig. 1: from the sub-nanoscale $(50-150\mathrm{nm})$ to the microscale $(10-500\mu\mathrm{m})$ where cortical bone tissue is considered.

The direct homogenization (DH) procedure by means of the finite element method (FEM), the continuum approach based on the Hill bounds, the

least-square method and the mean field technique are the fundamentals of the methodology of this analysis. Firstly, the volumetric content of the different components in each phase is described. These parameters are related to the volumetric bone mineral density (BMD) since the bone mineralization process occurs at the smallest scale length of the bone tissue. The following definitions have been considered:

- **Fibril**: staggered distribution of collagen molecules in a 5-D period arrangement (Hodge et al., 1963; Landis et al., 1993; Silver and Landis, 2011). Hierarchical mineralization takes place at the gap zones within the collagen scaffold (Liu, 2011). In our work, the microfibrils (a pentameric collagen molecules arrangement in a quasi-hexagonal pattern (Orgel et al., 2006)) are encompassed in the fibrils.
- **Fibre** or **Fibrils assembly**: Fibrils bounded to conform a major structure with transversely isotropic behavior. The work of Rubin et al. (2003) has been considered at this point.
- **Fibre array**: Combination of fibres (reinforcement) with extra-fibrilar matrix. In this work an hexagonal distribution of fibres is assumed. Similar notation is adopted in Reisinger et al. (2011).

2.2 Parameters description

In the subsequent procedure the term V_{comp}^{phase} represents the volume of a component *comp* in a *phase* per unit volume of bone tissue. If *phase* is not specified, V_{comp} represents the volume of the *comp* per unit volume of bone tissue. If

comp is not specified, V^{phase} represents the total volume of the *phase* per unit volume of bone tissue. By analogy to structural composite materials, two *phases* can be distinguished in lamellar bone tissue, the fibres (fibrils-assembly) and extra-fibrilar matrix, therefore:

$$V^{fib} + V^{mat} = 1 \tag{1}$$

Following Fritsch and Hellmich (2007) the volume of fibres per unit volume of bone tissue is considered a fixed value $V^{fib} = 0.53$.

Neglecting the volatile inorganic substances and cells, the main components of bone tissue are Type I collagen molecules, V_{col} (organic phase), mineral, V_{min} (hydroxyapatite crystals and amorphous phase) and water, V_{water}, therefore:

$$V_{col} + V_{min} + V_{water} = 1 \tag{2}$$

Collagen, water and crystals of mineral are within the fibrils whereas the main components of the extra-fibrilar matrix are amorphous mineral and water (neglecting non-collagenous proteins).

In this work the content of collagen has been considered constant assuming the value proposed by Yoon and Cowin (2008a) for cortical bone: $V_{col} = 0.354$.

In Table 1 the distribution of the main bone tissue components (collagen, mineral and water) in the phases (fibres and extra-fibrilar matrix) are summarized.

The volumetric bone mineral density BMD ($\mathrm{gr/cm^3}$) represents the mineral mass, m_{min}, per unit volume of tissue: $BMD = \dfrac{m_{min}}{vol_{tissue}}$. Hence, the volume

Table 1 *Distribution of the main bone tissue components (collagen, mineral and water) in the phases (fibrils and extra-fibrilar matrix). The volume fraction per unit volume of bone tissue of the phases is assumed constant in this work,* $V^{fib} = 0.53$ *(Fritsch and Hellmich, 2007)*

	Phases	
	Fibres ($V^{fib} = 0.53$)	*Extra-fibrilar matrix* ($V^{mat} = 0.47$)
Components	Collagen	—
	Crystals of mineral	Amorphous mineral
	Water	Water

of mineral per unit volume of bone tissue V_{min} can be expressed in terms of BMD by the following equation:

$$V_{min} = \frac{vol_{min}}{vol_{tissue}} = \frac{BMD}{\rho_{min}} \tag{3}$$

being $\rho_{min} = 3.12$ gr/cm^3 the mineral density (Lees et al., 1979).

From Eq. 2, the volume of water per unit volume of tissue is:

$$V_{water} = 1 - V_{col} - V_{min} \tag{4}$$

The following parameter α represents the ratio between intrafibrilar mineral and the mineral deposited in the whole lamellar bone tissue and will be a fixed value in this work, $\alpha = 0.23$ (Sasaki et al., 2002). Therefore, the volume of mineral within the fibres V_{min}^{fib} and the volume of mineral in the extrafibrillar matrix V_{min}^{mat}, both of them per unit volume of tissue, will be provided by the next equations:

$$V_{min}^{fib} = \alpha V_{min} \tag{5}$$

$$V_{min}^{mat} = (1-\alpha)\, V_{min} \tag{6}$$

Water is distributed within fibres and extrafibrilar matrix. Since all the collagen is within the fibres, $V_{col}^{fib} = V_{col}$, the following parameters definition arise:

$$V_{water}^{fib} = V^{fib} - V_{min}^{fib} - V_{col} \tag{7}$$

$$V_{water}^{mat} = V_{water} - V_{water}^{fib} \tag{8}$$

As mentioned at the beginning of Sec. 2.2, the variable V always denotes volumetric fraction per unit volume of bone tissue. Hereafter, the variable ϕ_{comp}^{phase} represents the volume of the component present in the phase, *comp*, per unit volume of the *phase*.

Up to this point, water has been considered explicitly. Subsequently, the volumetric fractions, ϕ, of the "dry" constituents in the fibril-array are defined as follow:

$$\phi_{water}^{fib} = \frac{vol_{water}^{fib}}{vol^{fib}} = \frac{V_{water}^{fib}}{V^{fib}} \tag{9}$$

$$\phi_{min}^{fib} = \frac{vol_{min}^{fib}}{vol^{fib}} = \frac{V_{min}^{fib}}{V^{fib}} \tag{10}$$

$$\phi_{col}^{fib} = 1 - \phi_{water}^{fib} - \phi_{min}^{fib} \tag{11}$$

Following the work of Martínez-Reina et al. (2011), from now on, water will be added to the rest of constituents that become wet constituents (wet-collagen and wet-mineral), which is a more realistic description. In this new context, the volumetric fraction of water is assumed to be the same in both wet-mineral and wet-collagen and equal to volumetric fraction of water within the

fibres. Thus, considering the new phases wet-collagen ($wcol$) and wet-mineral ($wmin$), this idea can be expressed:

$$\phi_{water}^{wcol} = \phi_{water}^{wmin} = \phi_{water}^{fib} \tag{12}$$

Accordingly, the ratio between the volumetric fraction of wet-mineral and the volumetric fraction of wet-collagen within the fibres must be equal to the same ratio expressed in dry components, thus the water within the fibres is distributed in the wet components preserving the dry proportions:

$$\frac{\phi_{wmin}^{fib}}{\phi_{wcol}^{fib}} = \frac{\phi_{min}^{fib}}{\phi_{col}^{fib}} \tag{13}$$

and, additionally, the components of the fibres become wet-mineral and wet-collagen:

$$\phi_{wmin}^{fib} + \phi_{wcol}^{fib} = 1 \tag{14}$$

From Eqs. 13 and 14, the above two equations, the volumetric fractions of the wet components within the fibril can be worked out:

$$\phi_{wmin}^{fib} = \frac{\phi_{min}^{fib}}{\phi_{min}^{fib} + \phi_{col}^{fib}} \tag{15}$$

and, by substitution:

$$\phi_{wcol}^{fib} = 1 - \phi_{wmin}^{fib} = \frac{\phi_{col}^{fib}}{\phi_{min}^{fib} + \phi_{col}^{fib}} \tag{16}$$

The same approach can be considered for the extra-fibrillar matrix and its water content: considering the extrafibrilar matrix as a mineral-water composite, the volume fractions of the components within the extrafibrilar matrix are:

$$\phi_{min}^{mat} = \frac{V_{min}^{mat}}{V^{mat}} \tag{17}$$

$$\phi_{water}^{mat} = 1 - \phi_{min}^{mat} \tag{18}$$

where V_{min}^{mat} is provided by Eq. 6.

At this point, a relationship between the BMD and the volumetric fraction of wet-mineral within the fibril ϕ_{wmin}^{fib} can be derived:

Deriving BMD from Eq. 3 and substituting V_{min} from Eq. 5:

$$BMD = V_{min}\rho_{min} = \frac{V_{min}^{fib}}{\alpha}\rho_{min} \tag{19}$$

replacing V_{min}^{fib} from Eq. 10:

$$BMD = \frac{V^{fib}\phi_{min}^{fib}\rho_{min}}{\alpha} \tag{20}$$

The volumetric fraction of collagen within the fibres is:

$$\phi_{col}^{fib} = \frac{V_{col}^{fib}}{V^{fib}} \tag{21}$$

Therefore, working out V^{fib} from Eq. 21 and substituting in Eq. 20:

$$BMD = \frac{V_{col}^{fib}\rho_{min}}{\alpha}\frac{\phi_{min}^{fib}}{\phi_{col}^{fib}} \tag{22}$$

Finally, from Eqs. 13 and 14:

$$BMD = \frac{V_{col}^{fib}\rho_{min}}{\alpha}\frac{\phi_{wmin}^{fib}}{1-\phi_{wmin}^{fib}} \tag{23}$$

Note that $V_{col}^{fib} = 0.354$ is assumed a constant value and α, the intrafibrilar - mineral tissue ratio, is fixed in this work. Hence, the wet-mineral within the fibre ϕ_{wmin}^{fib}, that is considered in the finite element models of the fibril, is directly related with the BMD.

2.3 Sub-nano and nanoscale

At the sub-nanoscale length ($50 - 150$nm), the main constituents of bone tissue are: Type I collagen macromolecules, hydroxyapatite crystals of mineral (platelet-shaped), amorphous mineral and water. At the nano-scale length ($300\text{nm} - 1\mu m$), two phases will be differentiated where the main constituents cited above are distributed: (1) the mineralized collagen fibrils, that are assembled into fibres (fibrils assembly), contain all the collagen, platelet-shaped minerals and water, and (2) the extra-fibrilar matrix that contains amorphous mineral and water.

2.3.1 Mineralized collagen fibril. Fibres

Following the work of Martínez-Reina et al. (2011), the mineralized collagen fibrils are composed by wet-collagen and wet-mineral. The isotropic elastic constants for the wet components within the fibrils that are used in this work are: $E_{col} = 1.2$GPa, $\nu_{col} = 0.35$ for wet-collagen and $E_{min} = 114$GPa, $\nu_{min} = 0.28$ for wet-mineral.

Within the fibrils, adjacent collagen molecules are arranged in a D-periodic sequence ($D = 67$nm) (Hodge et al., 1963) that provides the scaffold for the further hierarchical intrafibrilar mineralization. The crystals of mineral are platelet-shaped and the dimensions of the platelets are represented by $L \times W \times T$ being the distance between them: d_L, d_W and d_T. In this work, the finite element method is used to analyze a parameterized unit cell of a fibril of dimensions $a \times b \times c$, being $a = L + d_L$, $b = W + d_W$ and $c = 5(T + d_T)$

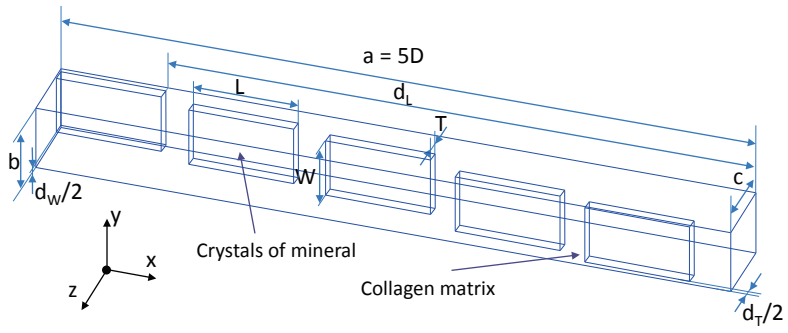

Fig. 2 Three dimensional view of the mineralized collagen fibril unit cell ($a \times b \times c$) and principal dimensions of the domain (reprinted from Vercher-Martínez et al. (2015) with permission of Elsevier)

Table 2 *Ranges and averaged values for platelet dimensions L, W and T*

Reference	L	W	T
Landis et al. (1993)	40-170nm	30-45nm	4-6nm
Rubin et al. (2003) (normal bone)	50.7±9.1nm	27.2±3nm	1.5±7.7nm
Robinson et al. (1952) (cortical bone)	20-150nm	10-80nm	8-15nm
Rho et al. (1998) (average values)	50nm	25nm	3nm

(see Fig. 2). This model presents a period of $5D$ in the longitudinal direction (Cowin, 2000). Collagen is modelled by a continuous matrix and the platelet-shaped mineral are located in the gap collagen zones (Silver and Landis, 2011; Fratzl et al., 1991) forming parallel layers. A detailed explanation of the numerical model of the mineralized collagen fibril is given in Vercher-Martínez et al. (2015).

In literature, there is a wide range of values for platelet dimensions. A summary is presented in Table 2.

According to Bar-On and Wagner (2013), the ratio $W/(W+d_W)$ (see Fig. 2) is usually considered approximately 1 because in many biological configurations the platelets are tightly packed. Hence, in this work, the fixed values $W = 30$nm and $d_W = 2$nm are assumed. With these considerations and being $L + d_L \approx 5D$, the volumetric fraction of wet-mineral within the fibril can be estimated through the following equation (Akiva et al., 1998; Vercher et al., 2014):

$$\phi_{wmin}^{fib} = \frac{LW}{5D(W + d_W)\left(1 + \frac{d_T}{T}\right)} \tag{24}$$

According to the model of mineralized collagen fibril proposed in this work, the volumetric fraction of wet-mineral in the gap collagen zone is obtained by means of:

$$\phi_{wmin}^{fib,gap} = \frac{T}{c} = \frac{1}{5\left(1 + \frac{d_T}{T}\right)} \tag{25}$$

In this work, the minimum lateral distance is fixed in $d_T = -1$nm which, substituting in Eq. 25, leads to a $\phi_{wmin}^{fib,gap} = 0.25$, lower than the upper possible limit established in Jäger et al. (2000). Therefore, in this study, the distance d_T is varied within the range $[-1, 3]$nm in increments of 1nm.

Regarding the platelet thickness, the fixed value $T = 5$nm is chosen in this work in agreement with the values proposed in the literature.

Moreover, the platelets grow across the fibril forming grooves or channels (Weiner and Traub, 1986; Landis et al., 1993). Hence, in order to avoid contact between platelets, the maximum mineral length L should be constrained by the lateral distance d_T (see Fig. 3). Therefore, if $d_T \leq 0$ (lateral mineral overlap exists), then, the maximum mineral length should be $L_{max} = 66$nm to avoid

Table 3 *Maximum volumetric fraction of mineral within the fibril for different proportions of platelet overlap. Models number*

$\frac{d_T}{T}$	-0.2	0	0.2	0.4	0.6
L	$[40, 50, 60, \mathbf{66}]$nm		$[40 - \mathbf{150}]$nm inc. of 10nm		
Models	1-4	5-8	9-20	21-32	33-44
Maximum ϕ_{wmin}^{fib}	0.231	0.185	0.350	0.300	0.262

mineral contact and if $d_T > 0$ then L_{max} should be 150nm (Robinson et al., 1952).

As it was mentioned previously, the volumetric fraction of wet-mineral within the fibril can be estimated by means of Eq. 24. In this work, the variable parameters of this equation are L and d_T because they are the most influent in the estimation of the volumetric mineral fraction within the fibril, the last as a consequence of the high and non-linear relationship and the former because the large range of values reported in literature. Table 3 summarizes the procedure followed to obtain the numerical models of the fibrils: the parameter $\frac{d_T}{T}$ varies from -0.2 to 0.6. For each value of $\frac{d_T}{T}$, a range of values of L is analyzed considering the geometrical restriction of avoiding mineral contact: L has been varied in $[40, 50, 60, 66]$nm for $d_T \leq 0$ and in the range $[40-150]$nm in increments of 10nm for $d_T > 0$. All these combinations correspond to 44 numerical models. Then, for a given $\frac{d_T}{T}$, the maximum volumetric fraction of wet-mineral within the fibril can be estimated by means of Eq. 24 considering the maximum length L within each range (marked in bolt in Table 3).

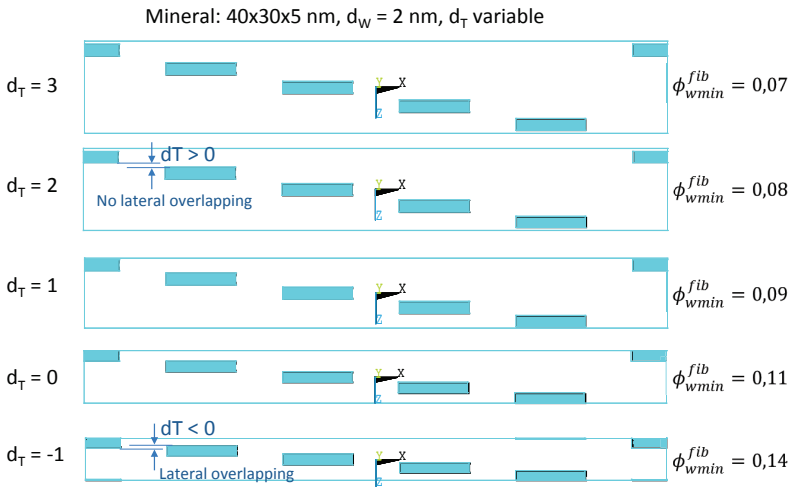

Fig. 3 Example of some unit volumes analyzed by the finite element method for different lateral space between minerals, $d_T \in [-1, 3]$nm. Dimensions W, T and d_W remain constant. In this figure, $L = 40$nm. The mineral is represented in blue and collagen in white

In Fig. 3 a sequence of some models analyzed by means of finite elements, shows the increasing level of mineral compaction as d_T is reduced and thus, the volumetric fraction of mineral within the fibril. In this figure, the values of L, W, T and d_W are fixed.

On the other hand, some values of the maximum volumetric fraction of wet-mineral within the fibril are provided in the literature: 0.238 (Martínez-Reina et al., 2011), 0.3 (Reisinger et al., 2011; Fritsch and Hellmich, 2007). Accordingly, the maximum $\phi^{fib}_{wmin} = 0.3$ is assumed in this work, hence a total of 42 models have been selected from the 44 models described in Table 3.

In order to estimate the stiffness matrix $\mathbf{C}$ of the mineralized collagen fibril, six canonical load cases are applied with periodic boundary conditions (see equations in Vercher-Martínez et al. (2015)). These conditions allow to

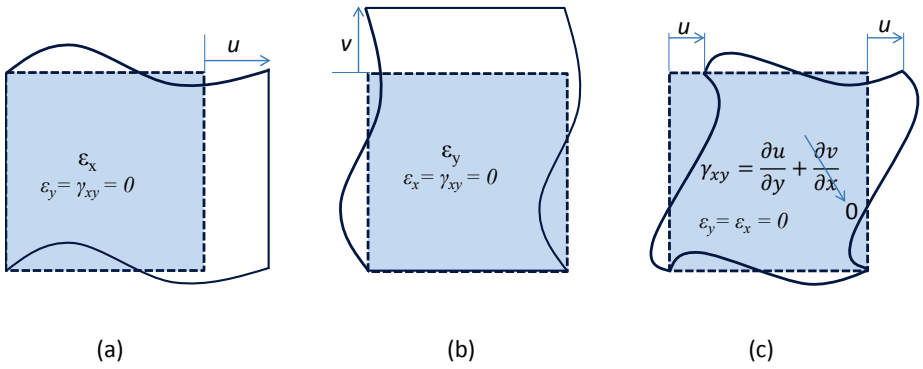

Fig. 4 Schematic representation of the load cases with periodic boundary conditions in orthogonal directions of the elongation load cases (a), (b) and in the longitudinal direction for the shear load case (c). In this work, the periodic boundary conditions have been generalized for the three-dimensional problem

simulate an infinitely large fibril (see the schematic representation for the bi-dimensional problem in Fig. 4). A total of 252 numerical analysis were performed considering the 42 models that accomplish $\phi^{fib}_{wmin} \leq 0.3$. The solution is the monoclinic stiffness matrix of every numerical model of a single fibril.

Besides, the platelets can rotate around its own crystallographic c-axis inside the fibril whilst the fibril orientation in the lamellar tissue does not necessarily vary (angle Ψ_2 in Fig. 5(b)). Considering the TEM (Transmision Electron Microscopy) observations reported by Rubin et al. (2003), the plateled-shaped crystals rotate around the c-axis in a circular pattern of 100-200nm (see Fig. 5(c)). This allows us to expect an averaged influence of Ψ_2 for a given set of unidirectional fibrils assembly (fibres). Hence, the monoclinic behavior (Vercher et al., 2014) of a single mineralized collagen fibril (see Fig. 5(a))

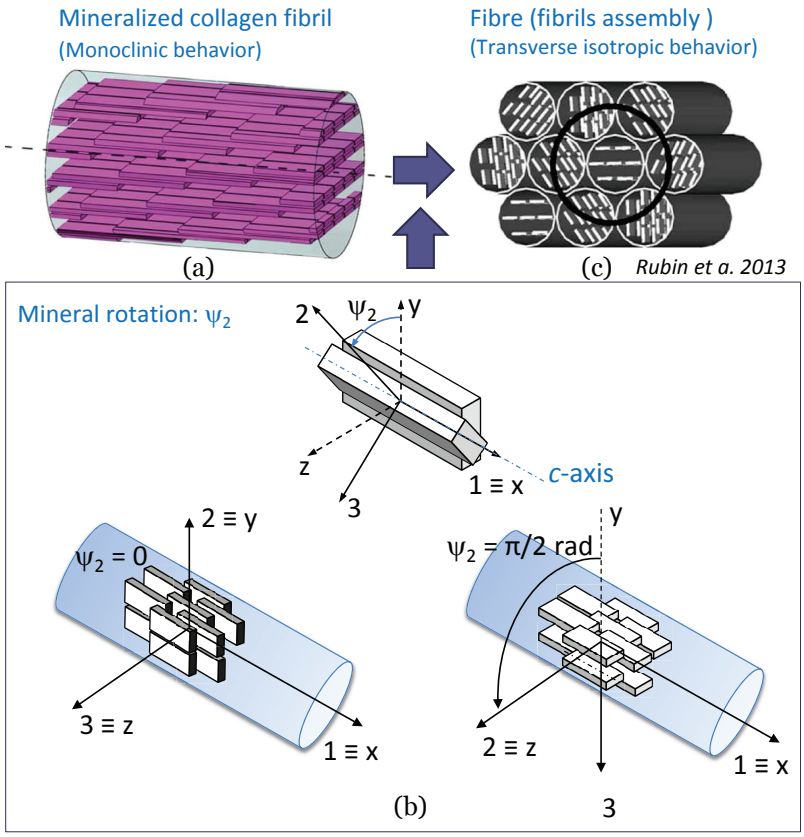

Fig. 5 (a) Hierarchical mineralization of single collagen fibril, (b) schematic representation of the platelet rotation Ψ_2 around its own $c-$axes, (c) schematic representation of the platelet rotation within 200nm region. Subfigures (a) and (b) are reprinted from Vercher-Martínez et al. (2015) with permission of Elsevier. Subfigure (c) is reprinted from Rubin et al. (2003) with permission of Elsevier

becomes a transversely isotropic behavior (Weiner and Wagner, 1998; Vercher-Martínez et al., 2015) for a fibre.

The upper and lower bounds (Hill, 1952) of the elastic properties of the fibril assembly will be calculated by averaging the compliance matrices in the

Ψ_2 range $[0, 2\pi]$:

$$\mathbf{C}_{\text{Upper}} = \frac{1}{2\pi} \int_0^{2\pi} \mathbf{q}\left(\Psi_2\right)^{\text{T}} \mathbf{C}\, \mathbf{q}\left(\Psi_2\right)\, \text{d}\Psi_2 \tag{26}$$

$$\mathbf{S}_{\text{Lower}} = \frac{1}{2\pi} \int_0^{2\pi} \mathbf{q}\left(\Psi_2\right)^{T} \mathbf{S}\, \mathbf{q}\left(\Psi_2\right)\, \text{d}\Psi_2 \tag{27}$$

where $\mathbf{q}\left(\Psi_2\right)$ is the Lekhnitskii's transformation matrix (Lekhnitskii, 1963), $\mathbf{C}$ and $\mathbf{S}$ are the stiffness and compliance matrices of the mineralized collagen fibril, obtained from the finite element analysis and Ψ_2 is the angle that mineral rotates about its own c-axis depicted in Fig. 5(b). This procedure has been applied to every monoclinic stiffness matrix of a single fibril.

2.3.2 Extra-fibrilar matrix

In this work, the extra-fibrilar matrix is considered a mineral-water composite (Martínez-Reina et al., 2011). Non-collagenous matrix proteins are neglected. The mineral present in the extra-fibrilar matrix is an amorphous phase that contains more water than apatite. This amorphous mineral will transform into a more compactly-packed apatite within the fibril (Liu, 2011). The isotropic elastic properties for the amorphous mineral are: Young's modulus $E_{amin} =$ 80GPa and the Poisson's ratio $\nu_{amin} = 0.28$ (Yuan et al., 2011). The following isotropic elastic properties for the water are considered: the bulk modulus $K_w = 2.3 \times 10^9$Pa and Poisson's ratio $\nu_w = 0.4998$ (almost incompressible) (Martínez-Reina et al., 2011).

Therefore, Hill bounds are estimated for the mineral-water composite through:

$$\mathbf{C}^V_{mw} = \mathbf{C}_{amin}\phi^{mat}_{min} + \mathbf{C}_w(1 - \phi^{mat}_{min}) \tag{28}$$

$$\mathbf{S}^R_{mw} = \mathbf{S}_{amin}\phi^{mat}_{min} + \mathbf{S}_w(1-\phi^{mat}_{min}) \tag{29}$$

where $\mathbf{C}_{mw}$ and $\mathbf{S}_{mw}$ are the stiffness and compliance matrix of the mineral-water composite. V and R represent the classical Voigt and Reuss bounds. The upper and lower bound of the shear modulus and the bulk modulus, (μ^V_{mw}, K^V_{mw}) and (μ^R_{mw}, K^R_{mw}) are then averaged. The volumetric fraction of mineral in the matrix, ϕ^{mat}_{min}, is calculated by means of Eq. 17. Note that ϕ^{mat}_{min} is a function of the BMD through Eq. 3 and 6:

$$\phi^{mat}_{min} = \frac{V^{mat}_{min}}{V^{mat}} = \frac{(1-\alpha)\,\frac{BMD}{\rho_{min}}}{V^{mat}} \tag{30}$$

where $V^{mat} = 1 - V^{fib} = 0.47$.

2.4 Sub-microscale

At the sub-microscale length $(1-10\mu m)$, the lamellar bone is established. This tissue is composed by fibres (mineralized collagen fibrils assembly) with transversely isotropic behavior (see Sec. 2.3.1) and the isotropic extra-fibrilar matrix (see Sec. 2.3.2). The procedure to analyze the sub-microscale length in the multiscale approach is the following: a representative unit cell of the lamellar tissue is modelled assuming a hexagonal regular packaging of the fibres within the extra-fibrilar matrix (Rubin et al., 2003), see Fig. 6. The volumetric fraction of the fibre in this model is 0.53 (according to Fritsch and Hellmich (2007) as commented in Sec. 2.2). In the numerical analysis, a refined mapped mesh of linear hexahedra has been considered.

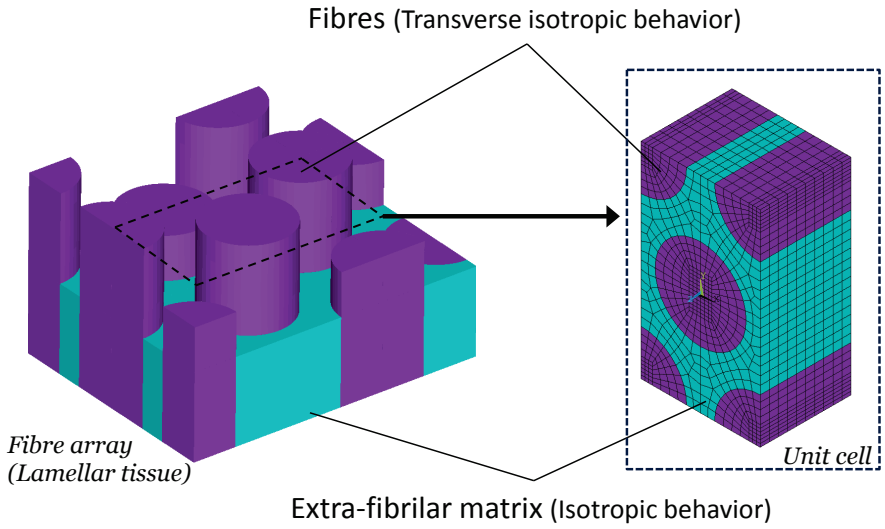

Fig. 6 Model of a unit cell of lamellar tissue. The fibres are distributed in a hexagonal regular distribution with a volume faction of 0.53 (Fritsch and Hellmich, 2007)

Table 4 *Values of BMD for which numerical results are obtained for the elastic constants of lamellar tissue*

BMD(gr/cm^3)								
0	0.36	0.73	1.10	1.23	1.4	1.57	1.8	1.9

Subsequently, the direct homogenization procedure is applied to estimate the stiffness matrix of the unit lamellar tissue for the nine discrete values of BMD shown in Table 4.

For each point, a numerical model of fibre array is analyzed. Then, the least square method is used to provide the explicit expressions of the five elastic constants of the lamellar tissue as a function of the BMD.

2.5 Microscale

Lamellar tissue is the main structural unit of bone. Mature cortical bone is composed by a calcified interstitial matrix and secondary osteons. In the latter, the lamellar tissue is arranged in concentric layers around the Haver's canal forming the lamellae. Beside the rotation ψ_2 described in Sec. 2.3.1, the crystals of the mineralized collagen fibrils change their orientation (angle ψ_1 in Fig. 7) and, as a consequence, the longitudinal direction of the fibril also changes. This occurs across the whole osteon. Note that this rotation is around a radial axis of the osteon, hence the c-axis of the minerals is always contained in a tangential plane. On the other hand, the outer layer of the osteon is the cement line ($\sim 2\mu m$ in thickness), that will be considered an isotropic material with $E_{cl} = 88.5$MPa and $\nu_{cl} = 0.25$ (Nobakhti et al., 2014).

Fig. 8 represents the orientation arrangement of the fibrils with the normalized radial coordinate, ξ, from Wagermaier et al. (2006). This pattern has been adopted in the current work. As described in Reisinger et al. (2011), the origin for the angle θ in Fig. 8 is the longitudinal direction of the osteon, then the rotation ψ_1 is $\psi_1 = \theta + 90°$.

Additionally, in the present work, the variation of the BMD described in Granke et al. (2013) is considered as a particular case. In that work the bone mineral density in an osteon was quantified by means of Synchrotron Radiation-μCT. A lower BMD is observed in the inner layer (1.02 ± 0.06 gr/cm^3) compared with the peripheral layer (1.16 ± 0.04 gr/cm^3).

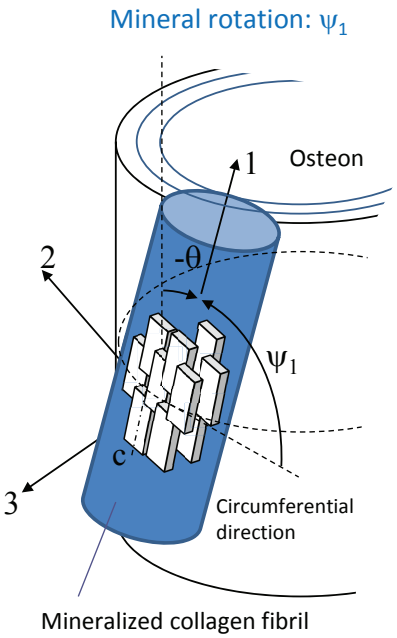

Fig. 7 Schematic representation of the ψ_1 rotation

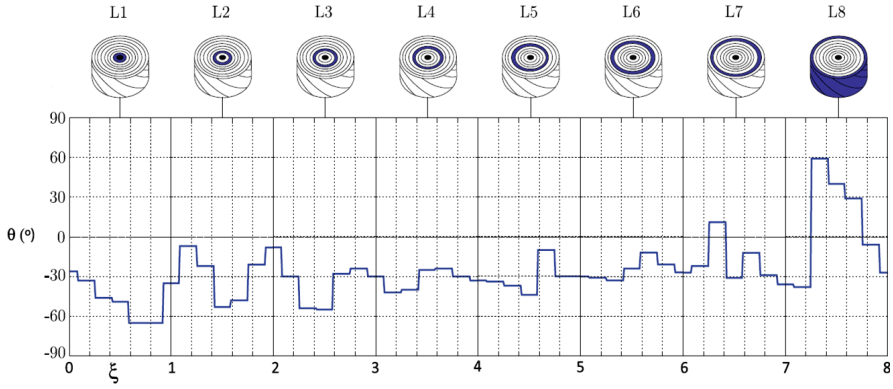

Fig. 8 Fibril orientation pattern across an osteon (normalized coordinate ξ) observed in Wagermaier et al. (2006). Reprinted from Wagermaier et al. (2006) with permission of Elsevier

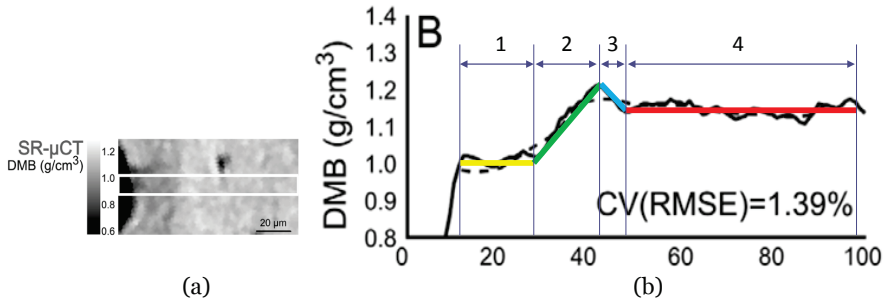

Fig. 9 (a) BMD distribution across an osteon, from Granke et al. (2013) (b) Straight lines fitted to the Granke's curve in this work

Table 5 *Averaged values of BMD within each portion delimited by* $[r_i - r_e]$

Material	$[r_i - r_e]\mu$m	BMD(gr/cm^3)
1	[25-34.4]	1.02
2	[34.4-41.7]	1.13
3	[46.7-44.8]	1.19
4	[44.8-73]	1.15

In Fig. 9 (a) an illustration from Granke et al. (2013) is reprinted and in (b) the treatment adopted in the current work is shown where four straight lines are fitted to the Granke's curve (see Table 5).

In order to estimate the elastic constants of the cortical bone, a unit cell is modelled by the finite element method. In Fig. 10(a) a scheme of the region of interest analyzed is shown. The diameter of the osteon is considered 150μm and the Haver's canal, 50μm (Cowin, 2001). In Fig. 10(b) a detail of the mapped mesh (on the plane xy) is depicted. A total of 54 layers are generated with

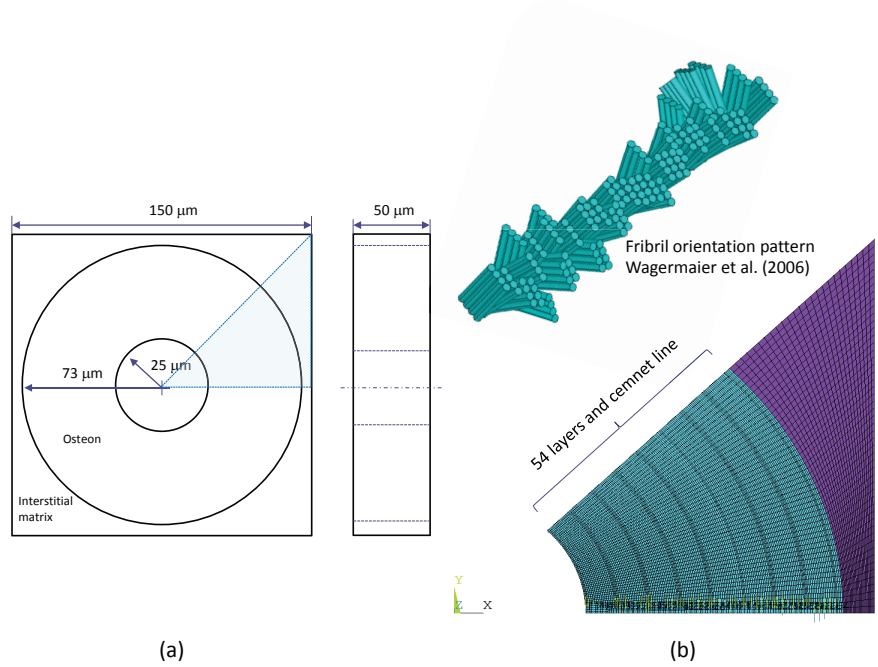

Fig. 10 (a) Scheme of the unit cell of cortical bone (b) Mesh detail of the numerical model of the cortical bone. User coordinate systems are used to define the elastic constants of transversely isotropic lamellar tissue. Above illustration of the fibril orientations implicitly modelled

user coordinate systems to define the transversely isotropic behavior of the lamellar tissue (see Sec. 2.4).

In Fig. 11, the different colors in the osteon correspond to different material properties, depending on the mineral content.

Finally, the interstitial matrix is assumed isotropic with $E_{imat} = 13.73$GPa and $\nu_{imat} = 0.3$ (Nobakhti et al., 2014). A direct homogenization procedure is again applied to estimate the stiffness matrix of cortical bone.

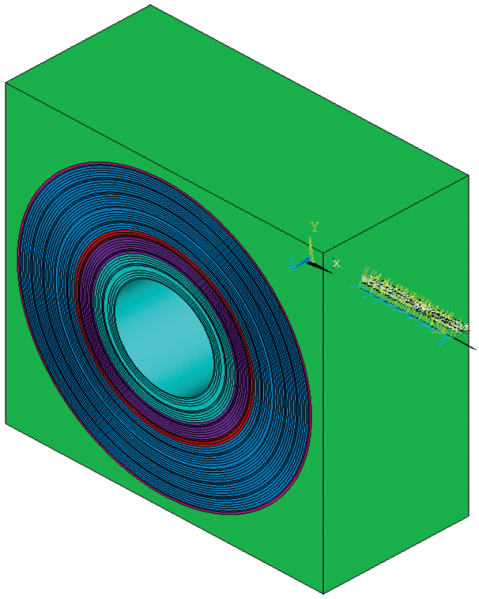

Fig. 11 Materials assignment into the numerical model

3 RESULTS

3.1 Nano-scale: fibres and extra-fibrilar matrix

The numerical model for fibrils assembly proposed in Vercher-Martínez et al. (2015) are considered as a starting point. In the present work the parameters that define the distribution of the main constituents of bone are also included (see Sec. 2.2). In addition, the statistical treatment of the results obtained from the numerical models of the fibril has enabled to fit non-linear regressions that predict the transversely isotropic behavior of the fibrils assembly as a function of the BMD. Another contribution is that the extra-fibrilar matrix analysis is also included.

The following regressions provide the transversely isotropic elastic constants of the fibrils assembly (fibre) for $BMD < 2$ gr/cm^3. The axis definition is depicted in Fig. 3. Note that the longitudinal direction of the fibres in these equations corresponds with the x direction.

$$E_x^{fib} = 10^9(5BMD^{1.8} + 1.2);\ R^2 = 0.92 \tag{31}$$

$$E_y^{fib} = 10^9(1.36BMD^{0.73} + 1.2);\ R^2 = 0.99 \tag{32}$$

$$\nu_{xy}^{fib} = 0.049BMD^2 - 0.121BMD + 0.34;\ R^2 = 0.78 \tag{33}$$

$$\nu_{yz}^{fib} = -0.03BMD^2 + 0.093BMD + 0.35;\ R^2 = 0.92 \tag{34}$$

$$G_{zx}^{fib} = 10^8(4.85BMD^{0.93} + 4.44);\ R^2 = 0.95 \tag{35}$$

In Fig. 12, Eqs. 31-35 are represented in solid lines. The numerical results for the 42 numerical models described in Table 3 that accomplish with the condition $\phi_{wmin}^{fib} \leq 0.3$, are depicted with square markers.

On the other hand, the isotropic elastic constants for the extra-fibrilar matrix are estimated by means of Eqs. 28 and 29 were ϕ_{min}^{mat} is related with BMD according to Eq. 30. The elastic constants are evaluated at the discrete values of BMD shown in Table 4.

3.2 Sub-microscale: lamellar tissue

The proposed explicit expressions to estimate the transversely isotropic behavior of lamellar tissue based on BMD are here provided (see methods in

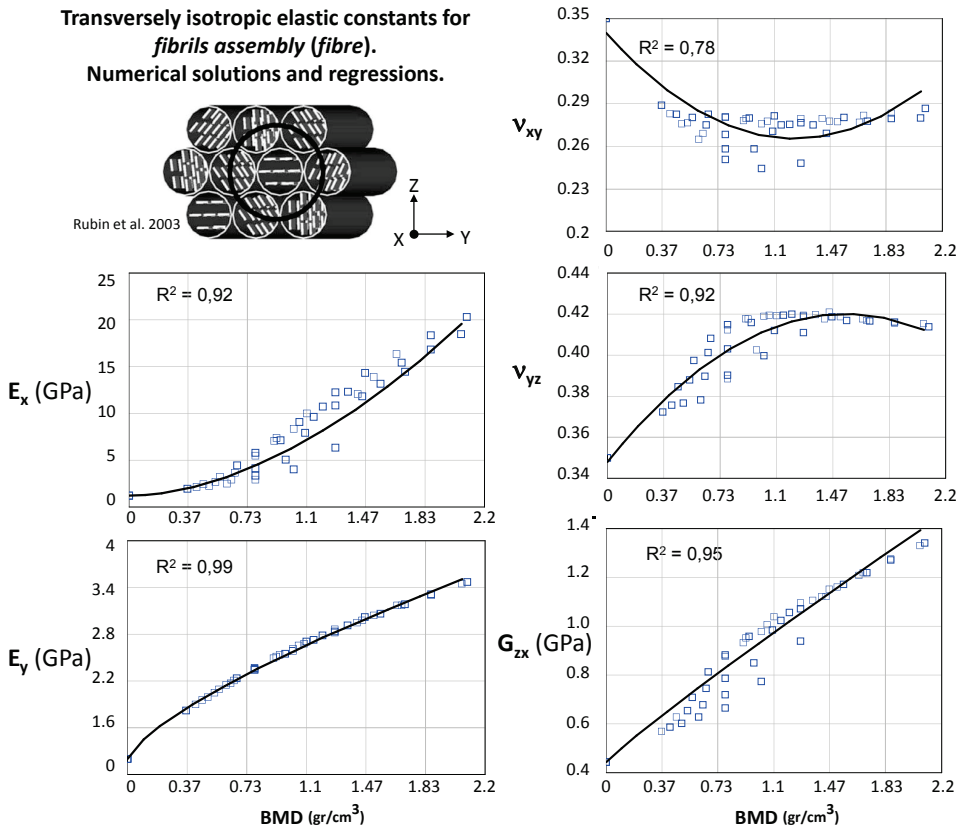

Fig. 12 Numerical results and regressions for the transversely isotropic elastic constants of the fibril assembly (fibre). The discrete finite element solutions are represented with square markers. The regressions correspond to Eqs. 31-35

Sec. 2.4). In this case, the equations that fit better to the numerical results obtained for Young's moduli and shear modulus are power regression.

$$E_x^{lam} = 10^7(770BMD^{0.8} + 1.54) \quad R^2 = 0.99 \tag{36}$$

$$E_z^{lam} = 10^8(130BMD^{1.2} + 6.4) \quad R^2 = 0.99 \tag{37}$$

$$\nu_{xy}^{lam} = \frac{0.6}{(1.1BMD + 1)^{10}} + 0.38 \quad R^2 = 0.99 \tag{38}$$

$$\nu_{yz}^{lam} = 0.253BMD^3 - 0.84BMD^2 + 0.77BMD + 0.01 \quad R^2 = 0.82 \tag{39}$$

$$G_{yz}^{lam} = 10^6(3300BMD^{0.9} + 3) \quad R^2 = 1 \tag{40}$$

In Fig. 13, the numerical results from the finite element analysis (marked as points) and the regressions (solid lines) show the evolution of the transversely isotropic elastic properties of lamellar bone with the BMD. Note the axis represented in the schematic plot. As it can be observed, the influence of the volumetric mineral content is noticeable for both Young's moduli and shear stiffness modulus being lower for Poisson's coefficients that tend to a constant value with increasing BMD.

The representative mean value of ratio between the Young's modulus in the longitudinal and transverse direction of the lamellar tissue is $\frac{E_z^{lam}}{E_x^{lam}} = 1.86$ (1.68 in Reisinger et al. (2010)). Following the procedure described in this work, the isolated influence of the BMD (Granke et al., 2013) in the estimation of the elastic constants of lamellar tissue (without the influence of the fibrils orientation), has been evaluated (see Fig. 14). In addition the elastic properties are also estimated considering a uniform value of BMD across the osteon radius: BMD= 1.2324 gr/cm^3 that corresponds to a $V_{min} = 0.395$ (Yoon and Cowin, 2008a).

If we consider the BMD distribution given by Granke et al. (2013) given in Fig. 9, the maximum variation of the mineral content can lead up to 3 GPa of difference in the longitudinal elastic modulus, up to 1 GPa of difference in the transversal elastic modulus, negligible influence in the Poisson's ratios and less than 1 GPa in the shear stiffness modulus. In case of considering the uniform

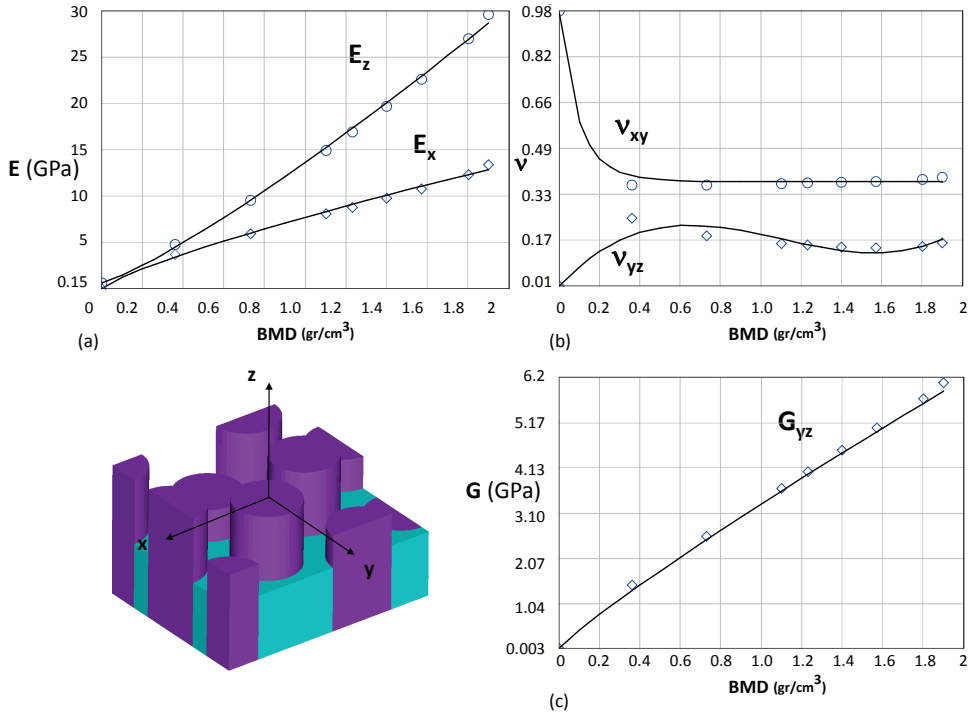

Fig. 13 Numerical results from the finite element analysis (with markers) and the regressions (in solid lines) of the transversely isotropic elastic constants of lamellar tissue as a function of BMD, (a) Young's moduli (Eqs. 36 and 37), (b) Poisson's ratios (Eqs. 38 and 39) and (c) shear stiffness modulus (Eq. 40)

value BMD = 1.2324 gr/cm^3 as the maximum, the differences are higher. This result highlights the dependency of the elastic constants of lamellar tissue with BMD.

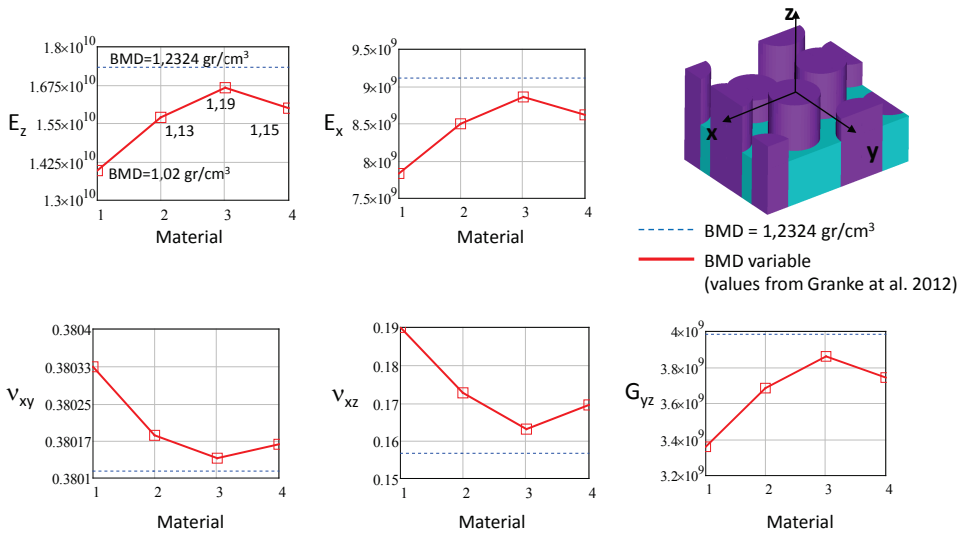

Fig. 14 Evolution of the elastic constants of lamellar tissue with BMD. The solid lines fit the discrete results corresponding with the different materials shown in Table 5 where the BMD changes. The dashed lines represent the results for the uniform value $BMD = 1.2324$ (gr/cm^3)

3.3 Microscale: cortical bone

The numerical procedure implemented allows us to apply the 6 canonical load cases preserving the periodic response of a cortical bone unit cell. The full stiffness matrix is then obtained. In this case, the cortical bone represented by the region of interest described in Sec. 2.5 is under consideration.

In Fig. 15 a table summarizes the elastic constants that are directly obtained from the numerical analysis. Influence coefficients and Chentsov's coefficients are negligible. Note that there is a wide range of variation in the elastic constant for cortical bone in literature. That can be observed even for

Elastic constants for a representative cell of cortical bone		
	BMD (Granke et al. 2012)	Uniform BMD *
E_x	3.26 GPa	3.26 GPa
E_y	3.26 GPa	3.26 GPa
E_z	13.00 GPa	13.76 GPa
ν_{xy}	0.097	0.099
ν_{xz}	0.067	0.063
ν_{yz}	0.067	0.063
ν_{yx}	0.097	0.099
ν_{zx}	0.265	0.266
ν_{zy}	0.265	0.266
G_{xy}	0.170 GPa	0.172 GPa
G_{yz}	1.072 GPa	1.072 GPa
G_{zx}	1.072 GPa	1.072 GPa

* BMD = 1.2324 gr/cm^3

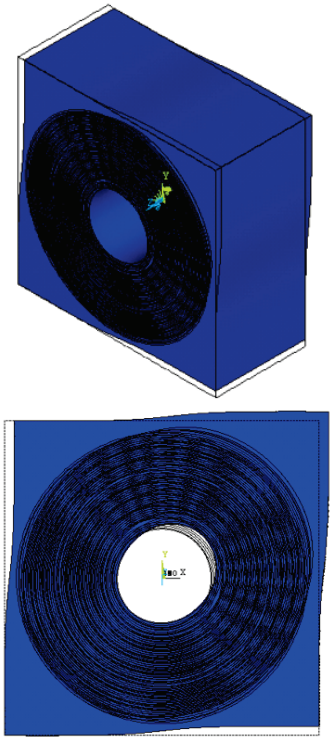

Fig. 15 Estimation of the elastic constants of cortical bone from the direct homogenization procedure by means of the finite element method (table). Two scenarios are considered, first the BMD distribution across the osteon observed by Granke et al. (2013) and second, the uniform value BMD = 1.2324 gr/cm^3. The figure illustrates the deformed shape for one of the six load cases imposed, γ_{xy}

the same type of bone. In Ascenzi and Bonucci (1967) the longitudinal stiffness is given for human osteons varying in the range: $[4.81 - 12.9]$GPa.

The non-isotropic behavior of the cortical bone is noticeable, being almost 4 times stiffer in the longitudinal than in the transverse direction of the osteon. As expected, the numerical results provide a transversely isotropic behavior of

the cortical bone being the plane xy the isotropic plane. The elastic constants obtained fulfill the thermodynamical restrictions (Lempriere, 1968; Gurtin, 1972; Vercher et al., 2014).

From these results, the BMD variation across the osteon does not seem to be very influent on the elastic constants obtained for cortical bone (see Fig. 15). Fibril orientation governs the anisotropic behavior of cortical bone much more than the mineral content. This result is in agreement with Granke et al. (2013).

However, the noticeable influence of the BMD on the elastic constants of lamellar tissue highlighted in Sec. 3.2, suggests that other tissues like cancellous bone, where lamellar tissue is formed in layers, would be more sensitive to the BMD variation than cortical bone. In this context, it is possible to relate the mineral content measured in cancellous bone with the BMD in lamellar tissue by means the following equation:

$$BMD_{cancellous} = \frac{BV}{TV} BMD_{lamellar} \tag{41}$$

where $\frac{BV}{TV}$ represents the bone volume fraction. From Eq. 41 the $BMD_{lamellar}$ can be worked out being function of the $\frac{BV}{TV}$ and $BMD_{cancellous}$ which, in turn, can be obtained from image analysis and μCT.

4 DISCUSSION AND CONCLUSIONS

In this work, explicit expressions to estimate the transversely isotropic behavior of lamellar bone are proposed. To achieve this goal, a multi-scale approach

is applied in accordance with the hierarchical structure of bone. The methods considered are direct homogenization procedure by finite element methods, continuum approach based on Hill bounds, least square method and mean field technique. In a preliminary analysis of the distribution of the main components of bone, the volumetric bone mineral density BMD is expressed as the independent variable. The rest of the parameters are fixed in accordance with the typical values found in literature. From this starting point, the results obtained in a previous work (Vercher-Martínez et al., 2015) for the transversely isotropic fibril assembly (fibres) are considered. However, several limitations of that work are currently addressed: the elastic constants of the fibre array or lamellar tissue are estimated as a function of the BMD by including the analysis of the extra-fibrilar matrix as a water-mineral composite. In addition, the proposed explicit expressions for the lamellar tissue are applied to cortical bone. In this case, the fibril orientation pattern described in Wagermaier et al. (2006) and the BMD distribution across an osteon presented in Granke et al. (2013) are considered.

It is remarkable that the transversely isotropic behavior of the fibrils assembly and hence, the lamellar tissue, is due to consider the full mineral rotation around its c-axis (Rubin et al., 2003) and the isotropic behavior of the extra-fibrilar matrix. If this is not the case, lamellar tissue exhibits an orthotropic behavior (Martínez-Reina et al., 2011) or monoclinic (Vercher-Martínez et al., 2015).

In the present study, a power regression for the Young's moduli of lamellar tissue as a function of BMD has been fitted. This result is in agreement with Currey (1986) where a power law for the relation between the apparent elastic modulus of cancellous bone and the $BMD_{cancellous}$ is reported. In addition, we provide the regressions for the rest of the transversely isotropic elastic constants.

From our results, a noticeable increment of the elastic moduli is observed with the increment of BMD. Similarly, in Martínez-Reina et al. (2011), the orthotropic Young's moduli of the lamellar tissue increase with the ash fraction. It is worth pointing out that the volumetric BMD map is obtained by dual-energy X-ray absorptiometry (DXA) (Yang et al., 2014) or computed tomography (QCT) (Majumdar et al., 1998) in the usual clinical practice, instead the ash fraction.

Regarding the analysis of cortical bone, the main source of porosity of cortical bone (Haver's canals) is explicitly modelled in this work. Other sources of porosity (canaliculi, lacunae, Volksmann's canals) have been neglected.

From the results obtained for the elastic constants of cortical bone, it can be concluded that the fibril orientation pattern across the concentric lamellar tissue in the secondary osteons governs the anisotropic behavior of cortical bone rather than the mineral content. However, the power regression for the lamellar tissue properties with BMD suggests that in other tissues like cancellous bone, the elastic constants may be more influenced by the mineral content. In this work, it is proposed a relationship between the BMD for lamellar

tissue, the BMD for cancellous bone and the $\frac{BV}{TV}$ ratio. Hence, transversely isotropic elastic properties for lamellar tissue can be derived instead of the typical isotropic elastic properties frequently assumed. We have verified that the volumetric bone mineral content BMD is a relevant parameter in order to improve the accuracy of the estimation of the lamellar bone elastic properties and we provide explicit expressions that correlate them.

This work presents several limitations. It could be necessary to include some weight factors in order to discerner what models of the fibrils are the most probably in the living tissue. Moreover, no sensitivity analysis of the parameters α (ratio between the intrafibrilar mineral content and the deposited in the lamellar bone) and V^{fib} (volume of fibres per unit volume of bone tissue) has been performed. In addition, when the Haversian system is analyzed, the isotropic elastic constants for the interstitial matrix can be substituted by more realistic values, in concordance with its own microstructure, this limitation will be overcome in a future work.

Currently, the authors are working on a model for the estimation of the elastic constants of lamellar tissue and cortical bone that includes the influence of the porosity due to osteoporosis. In addition, the proposed model for the transversely isotropic lamellar tissue is being applied to estimate the apparent elastic constants of cancellous bone.

Acknowledgements The authors acknowledge the Ministerio de Economía y Competitividad for the financial support received through the project DPI2013-46641-R and to the

Generalitat Valenciana for Programme PROMETEO 2016/007. The authors declare that they have no conflict of interest

References

Akiva U, Wagner HD and Weiner S (1998) Modelling the three-dimensional elastic constants of parallel-fibred and lamellar bone. J Mater Sci 33:1497-1509

Ascenzi A, Bonucci E (1967) The tensile properties of single osteons. Ana Rec 158:375-386

Barbour KE, Zmuda JM, Strotmeyer ES, Horwitz MJ, Boudreau R, Evans RW, Ensrud K, Petit MA, Gordon CL, Cauley JA (2013) Correlates of trabecular and cortical volumetric bone mineral density of the radius and tibia older men: the osteoporotic fractures in men study. J Bone Miner Res 25(5):1017-1028

Bar-On B, Wagner HD (2013) Structural motifs and elastic properties of hierarchical biological tissues - A review. J Struct Biol 183:149-164

Cowin SC (2000) How is a tissue built? J Biomech Eng 122:553-569

Cowin SC (2001) Bone Mechanics Handbook. Second Edition. CRC Press Boca Raton, Florida.

Currey JD (1986) Power law models for the mechanical properties of cancellous bone. Eng Med 15(3):153-154

Currey JD (1988) The effect of porosity and mineral content on the Young's modulus of elasticity of compact bone. J Biomech 21:131-139

Daszkiewicz K, Maquer G, Zysset PK (2017) The effective elastic properties of human trabecular bone may be approximated using micro-finite element analyses of embedded volume elements. Biomech Model Mechanobiol 16:731-742

Faingold A, Sidney RC, Wagner HD (2012) Nanoindentation of osteonal bone lamellae. J Mech Biomech Materials 9:198-206

Fratzl P, Fratzl-Zelman N, Klaushofer K, Vogl G, Koller K (1991) Nucleation and growth of mineral crystals in bone studied by small-angle x-ray scattering. Calcif Tissue Int 48:407-413

Fritsch A, Hellmich C (2007) 'Universal' microstructural patterns in cortical and trabecular, extracellular and extravascular bone materials: micromechanics-based prediction of anisotropic elasticity. J Theo Bio 24:597-620

Grampp S, Genant HK, Mathur A, Lang P, Jergas M, Takada M, Glüer CC, Lu Y, Chavez M, (1997) Comparisons of noninvasive bone mineral measurements in assessing age-related loss, fracture discrimination and diagnostic classification. J Bone Min Research 12:697-711

Grant CA, Langton C, Schuetz MA, Epari DR (2011) Determination of the material properties of ovine cortical bone. Poster No. 2226, 57th Orthopaedic Research Society (ORS) Annual Meeting, Long Beach, California.

Granke M, Gourrier A, Rupin F, Raum K, Peyrin F, Burghammer M, Saïd A, Laugier P (2012) Microfibril orientation dominates the microeslastic properties of human bone tissue at the lamellar length scale. Plos One 8, e58043.

Gurtin ME (1972) The linear theory of elasticity. Handbuch del Physik VIa/2:1-296

Hamed E, Jasiuk I (2012) Elastic modeling of bone at nanostructural level. Mat Sci Eng:R73:27-49

Hernández CJ, Beaupré GS, Keller TS, Carter DR (2001a) The influence of bone volume fraction and ash fraction on bone strength and modulus. Bone 29:74-78

Hill R (1952) The elastic behaviour of a crystalline aggregate. Proc Phys Soc Sec A 65:349-354

Hodge AJ, Petruska JA (1963) Recent studies with the electron microscope on ordered aggregates of the tropocollagen macromolecule. In: Ramachandran, GN (Ed.), Aspects of Protein Structure. Academic Press, New York, 289-300

Jäger I, Fratzl P (2000). Mineralized collagen: a mechanical model with a staggered arrangement of mineral particles. Bioph J 78:1737-1746

Kuhn JL, Goldstein SA, Choi K, London M, Feldkamp LA, Matthews LS (1989) Comparison of the trabecular and cortical tissue moduli from human iliac crests. J Orthopaedic Research 7:876-884

Landis WJ, Song MJ, Leith A, McEwen L, McEwen BF (1993) Mineral and organic matrix interaction in normally calcifying tendon visualized in three dimensions by high-voltage electron microscopic tomography and graphic

image reconstruction. J Struct Biol 110:39-54

Lees S, Heeley JD, Cleary PF (1979) A study of some properties of a sample of bovine cortical bone using ultrasound. Calcif Tissue Int 29:107-117

Lekhnitskii SG (1963) Theory of Elasticity of Anisotropic Elastic Body. Holden-Day San Francisco 1-73

Lempriere BM (1968) Poisson's ratio in orthotropic materials. Am Inst Aeronaut Astronaut J J6:2226-2227

Liu Y, Kim YK, Dai L, Li N, Khan SO, Pashley DH, Tay FR (2011) Hierarchical and non-hierarchical mineralization of collagen. Biomater 32:1291-1300

Majumdar S, Kothari M, Augat P, Newitt DC, Link TM, Lin JC, Lang T, Lu Y, Genant HK (1998) High-resolution magnetic resonance imaging: three-dimensional trabecular bone architecture and biomechanical properties. Bone 22(5):445-454

Martínez-Reina J, Domínguez J, García-Aznar JM (2011) Effect of porosity and mineral content on the elastic constants of cortical bone: a multiscale approach. Biomech Model Mechanobiol 10:309-322.

Nobakhti S, Limbert G, Thurner PJ (2014) Cement lines and interlamellar areas in compact bone as strain amplifiers - Contributors to elasticity, fracture thoughness and mechanotransduction. J Mech Behav Biomed Mater 29:235-251

Orgel JPRO, Irving TC, Miller A, Wess TJ (2006) Microfibrillar structure of type I collagn in situ. PNAS USA 103:9001-9005

Reisinger AG, Pahr DH, Zysset PK (2010) Sensitivity analysis and parametric study of elastic properties of unidirectional mineralized bone fibril-array using mean field methods. Biomech Model Mechanobiol 9:499-510

Reisinger AG, Pahr DH, Zysset PK (2011) Elastic anisotropy of bone lamellae as a function of fibril orientation pattern. Biomech Model Mechanobiol 10:67-77

Rho JY, Kuhn-Spearing L, Zioupos P (1998) Mechanical properties and the hierarchical structure of bone. Med Eng Phys 20:92-102

Robinson RA, Rochester MD (1952) An electron-microscopic study of the crystalline inorganic component of bone and its relationship to the organic matrix. J Bone Joint Surg 34-a: 389-435

Roque WL, Arcaro K, Alberich-Bayarri A (2013) Mechanical competence of bone: a new parameter to grade trabecular bone fragility from tortuosity and elasticity. IEEE Trans Bio Eng 60:1363-1370

Rubin MA, Jasiuk I, Taylor J, Rubin J, Ganey T, Apkarian RP (2003) TEM analysis of the nanostructure of normal and osteoporotic human trabecular bone. Bone 33: 270-282

Sasaki N, Tagami A, Goto T, Taniguchi M, Nakata M, Hikichi K (2002) Atomic force microscopic studies on the structure of bovine femoral cortical bone at the collagen fibril-mineral level. J Mater Sci Mater Med 13(3): 333-337

Schaffler MB, Burr DB (1988) Stiffness of compact bone: effects of porosity and density. J Biomech 21: 13-16

Silver FH, Landis WJ (2011). Deposition of apatite in mineralizing vertebrate extracellular matrices: A model of possible nucleation sites on type I collagen. Connective Tissue Research 52:242-254

Tommasini SM, Nasser P, Hu B, Jepsen KJ (2008). Biological co-adaptation of morphological and composition traits contributes to mechanical functionality and skeletal fragility. J Bone Miner Res 23:236-246

Ulrich D, Rietbergen B, Weinans H, Regsegger P (1998) Finite element analysis of trabecular bone structure: a comparison of image-based meshing techniques. Journal of Biomechanics 31:1187-1192

Ulrich D, Rietbergen B, Laib A, Regsegger P (1999) The ability of three-dimensional structural indices to reflect mechanical aspects of trabercular bone. Bone 25:55-60

Vercher A, Giner E, Arango C, Tarancón JE, Fuenmayor FJ (2014) Homogenized stiffness matrices for mineralized collagen fibrils and lamellar bone using unit cell finite element models. Biomech Model Mechanobiol 13:437-449

Vercher-Martínez A, Giner E, Arango C, Fuenmayor FJ (2015) Influence of the mineral staggering on the elastic properties of the mineralized collagen fibril in lamellar bone. J Mech Behav Biomed Mater 42:243-256

Wagermaier W, Gupta HS, Gourrier A, Burghammer M, Roschger P, Fratzl P (2006) Spiral twisting of fiber orientation inside bone lamellae. Biointerphases 1:1-5

Weiner S, Traub W (1986) Organization of hydroxiapatite within collagen fibrils. FEBS Lett 206:262-266

Weiner S, Wagner HD (1998) The material bone: structure-mechanical funtion relations. Annu Rev Mater Sci 28:271-298

Yang L, Palermo L, Black DM, Eastell R (2014) Prediction of incident hip fracture with the estimated femoral strength by finite element analysis of DXA scans in the study of osteoporotic fractures. JBMR 29:2594-2600

Yuan YJ, Cowin SC (2008a) The estimated elastic constants for a single bone osteonal lamella. Biomech Model Mechanobiol 7:1-11

Yu W, Glüer CC, Grampp S, Jergas M, Fuerst T, Wu CY, Lu Y, Fan B, Genant HK (1995) Spinal bone mineral assessment in postmenopausal women: a comparasion between dual X-ray absorptiometry and quantitative computed tomography. Osteoporosis Int 5:433-439

Yang L, Palermo L, Black DM, Eastell R (2014) Prediction of incident hip fracture with the estimated femoral strength by finite element analysis of DXS Scans in the study of osteoporotic fractures. J Bone Min Research 29(12):2594-2600

Yuan F, Stock SR, Haeffner DR, Almer JD, Dunand DC, Brinson LC (2011) A new model to simulate the elastic properties of mineralized collagen fibril. Biomech Model Mechanobiol 10:147-160

	Phases	
	Fibres ($V^{fib} = 0.53$)	*Extra-fibrilar matrix* ($V^{mat} = 0.47$)
Components	Collagen	—
	Crystals of mineral	Amorphous mineral
	Water	Water

Reference	L	W	T
Landis et al. (1993)	40-170nm	30-45nm	4-6nm
Rubin et al. (2003) (normal bone)	50.7±9.1nm	27.2±3nm	1.5±7.7nm
Robinson et al. (1952) (cortical bone)	20-150nm	10-80nm	8-15nm
Rho et al. (1998) (average values)	50nm	25nm	3nm

$\frac{d_T}{T}$	-0.2	0	0.2	0.4	0.6
L	$[40, 50, 60, \mathbf{66}]$nm		$[40 - \mathbf{150}]$nm inc. of 10nm		
Models	1-4	5-8	9-20	21-32	33-44
Maximum ϕ^{fib}_{wmin}	0.231	0.185	0.350	0.300	0.262

BMD(gr/cm^3)

0	0.36	0.73	1.10	1.23	1.4	1.57	1.8	1.9

Material	$[r_i - r_e]\mu$m	BMD(gr/cm^3)
1	[25-34.4]	1.02
2	[34.4-41.7]	1.13
3	[46.7-44.8]	1.19
4	[44.8-73]	1.15